Advanced Materials

ADVANCED MATERIALS
www.advmat.de

RESEARCH ARTICLE OPEN ACCESS

Boolean Logic-Based Control Over Recombinant Protein Biomaterial Degradability and Therapeutic Delivery

Murial L. Ross[1] | Ryan Gharios[2] | Shivani Kottantharayil[1] | Cole A. DeForest[1,2,3,4,5,6]

[1]Department of Bioengineering, University of Washington, Seattle, Washington, USA | [2]Department of Chemical Engineering, University of Washington, Seattle, Washington, USA | [3]Department of Chemistry, University of Washington, Seattle, Washington, USA | [4]Institute for Stem Cell & Regenerative Medicine, University of Washington, Seattle, Washington, USA | [5]Molecular Engineering & Sciences Institute, University of Washington, Seattle, Washington, USA | [6]Institute for Protein Design, University of Washington, Seattle, Washington, USA

Correspondence: Cole A. DeForest (profcole@uw.edu)

Received: 26 December 2025 | **Revised:** 16 June 2026 | **Accepted:** 24 June 2026

Keywords: biomaterials | boolean logic | controlled release | drugamer | recombinant proteins | stimuli-responsive

ABSTRACT

Recombinant protein-based biomaterials offer exciting opportunities in materials design and controlled therapeutic delivery. Though their precursors can be readily synthesized with near-perfect monodispersity and sequence specificity through scalable fermentation processes, recombinant protein materials have yet to achieve the same level of multi-stimuli-responsiveness as their synthetic counterparts. Integrating cutting-edge tools from chemical biology, we autonomously compile topologically specified protein crosslinkers that can be degraded following user-programmable Boolean logic. Covalent step polymerization of these linkers into protein hydrogels yields smart materials whose cargo (e.g., bioactive proteins, cellular therapeutics) can be liberated following bulk degradation in response to user-specified input combinations. Demonstrating the versatility of this approach, we release fluorescent protein mGreenLantern following all 17 possible YES/OR/AND logic outputs in response to a 3-input protease operator set, deliver epidermal growth factor following advanced biocomputation while maintaining native bioactivity, and showcase multiplexed delivery of living cells, all from fully recombinant protein-based hydrogels. Incorporating advanced intelligence into protein biomaterial responsiveness, we anticipate these methods will dramatically expand potential applications in tissue engineering and precision medicine.

1 | Introduction

Recombinant protein-based materials offer substantial promise for targeted drug delivery and tissue engineering applications [1–5]. Such proteins are encoded by DNA in a sequence-specified manner, affording a level of engineering control and reproducibility that is difficult to achieve with synthetic polymer-based systems [6–8]. Unlike their synthetic counterparts, genetically encoded polymers are comprised of the same building blocks found in living systems, allowing them to be easily formulated to be biocompatible, biodegradable, and bioinstructive [5–7, 9]. Moreover, protein material crosslinking can be carried out without harsh reagents or reaction conditions that risk denaturing biologics, an essential feature for constructs designed for protein or cell therapeutic release [10, 11]. Finally, the ability to genetically fuse or covalently conjugate protein therapeutics to the polymer backbone enables a flexible, modular platform that can be produced through scalable fermentation using equipment common in industrial bioprocessing. Despite these potential advantages, protein-based materials have lagged far

Murial L. Ross and Ryan Gharios contributed equally to this work.

behind their synthetic counterparts in terms of tunability and multi-stimuli-responsiveness [2, 6, 12, 13]. Though incorporation of stimuli-sensitive motifs within protein-based systems have yielded materials responsive to individual cues (e.g., shear strain [14–17], pH [18, 19], temperature [20–23], light [24–27], small molecule [28, 29], redox [30, 31]), those that precisely respond to preprogrammed input combinations of several stimuli have not been demonstrated.

To incorporate biocomputability into polymeric materials, our lab previously established that advanced Boolean-type responsiveness can be encoded into material systems through rational design of crosslinker topology [32, 33]. In this manner, a YES gate is formed when a single stimuli-degradable group is included within the crosslink that yields complete material dissolution when cleaved (Figure 1a,b). When two orthogonal stimuli-labile groups are connected in series within the crosslink, an OR gate (denoted with a logic symbol ∨) is formed such that cleavage of either moiety leads to bulk material degradation (Figure 1c). If the two scissile units are instead connected in parallel, both must be severed for material dissolution, forming the basis of an AND gate (denoted by a logic symbol ∧) (Figure 1d). Notably, more advanced logical operations can be encoded through hierarchical nesting of these YES, OR, and AND gates. When 3 inputs are employed, 17 unique signatures spanning 7 functionally distinct response types can be created (Figure 1e). These concepts have been demonstrated previously in poly(ethylene glycol) (PEG)-based materials crosslinked with synthetic peptides sensitive to enzyme, reducing agents, and/or light, though such peptide crosslinkers require several multi-step and low-yielding reactions that dramatically limit their scalable synthesis [32].

While molecular topology has been exploited previously to gain Boolean responsiveness over synthetic polymer-based systems, such methods have not yet been extended to protein materials, attributed primarily to the fact that proteins are predominantly linear constructs. Toward encoding biocomputation into protein systems, we recently demonstrated that topologically specified proteins can be formed during recombinant expression via orthogonal and spontaneous intramolecular ligation events [34]. In this manner, logically releasable protein cargos can be "autonomously compiled" prior to tethering to and subsequent release from synthetic polymer-based materials. Proteins from diverse functional classes (e.g., enzymes, nanobodies, cytokines) were then successfully delivered from synthetic gels and beads while maintaining native bioactivity [34, 35].

In this manuscript, we exploit autonomous compilation to construct topologically specified polypeptide crosslinkers that undergo covalent step polymerization into fully recombinant protein-based hydrogels whose bulk degradation and concurrent cargo release can be precisely programmed via Boolean logic. Material degradative outputs follow the expected logical signatures with high specificity in response to three orthogonal protease cues. To illustrate the versatility of this work, we control the release of bioactive epidermal growth factor (EGF) – "drugamer" species that are genetically encoded within the crosslinker itself – and encapsulated therapeutic cells. Collectively, this work establishes a modular, recombinant platform capable of executing programmable, multi-input therapeutic release with versatility and scalability beyond the reach of current synthetic polymer-based systems.

2 | Results and Discussion

2.1 | Crosslink Design, Purification, and Characterization

Prior work from our group established recombinant protein-based logical operators with single tethering points that allowed for tight control over protein release from synthetic materials [34, 35]. Inspired by these blueprints, we designed plasmid constructs for recombinant expression of 17 protein crosslinkers that collectively yielded all possible YES/OR/AND logic outputs from input combinations of 3 distinct proteases: sortase transpeptidase eSrtA(2A9) that can degrade LAET↓G (denoted as A) [36], human rhinovirus-3C (HRV-3C) protease which cleaves LEVLFQ↓GP (referred to as C) [37], and potyviral tobacco etch virus (TEV) protease which acts upon ENLYFQ↓S (denoted as T) [38, 39] (Figure 1f). All species were flanked with SpyTag motifs to permit covalent material crosslinking via SpyLigation, a genetically encoded "click" chemistry resulting in an isopeptide bond between the Tag and Catcher species [20, 40–43] (Figure 1g,h), as well as a 6x-histidine tag for nickel-NTA immobilized metal affinity chromatography (IMAC). To aid in the quantification of material degradation, all crosslinkers include mGreenLantern (mGL) [44], a monomeric green fluorescent protein variant evolved for enhanced brightness and expression levels.

The base operators were designed to autonomously compile within host cells as follows (Figure S1): (1) YES gates (i.e., A, C, T) contained one protease-specific recognition sequence between the flanking SpyTags and mGL. (2) OR gates (i.e., A∨C, A∨T, C∨T) contained two protease-cleavable sequences in series between the two SpyTags and mGL. (3) AND gates (i.e., A∧C, A∧T, C∧T) were cyclized using split-intein circular ligation of peptides and proteins (SICLOPPS) utilizing the Cfa intein system; when the split Cfa halves are respectively installed on a protein's N and C termini, the physically reassembled intein undergoes a rapid and near-scarless *trans*-splicing reaction that covalently cyclizes the interspaced protein while excising itself from the primary sequence [45, 46]. Additionally, a SsrA tag was installed at the C-terminus to tag all unspliced (i.e., non-cyclized) products for proteasomal degradation [47]. (4) (OR)AND-gated constructs [i.e., (A∨C)∧T, (A∨T)∧C, (C∨T)∧A] were assembled similarly to the AND structures via SICLOPPS, although the cyclized constructs contained two cleavable sequences in series with a third in parallel. (5) (AND)OR-gated constructs [i.e., (A∧C)∨T, (A∧T)∨C, (C∧T)∨A] have a tadpole-like geometry, necessitating macrocyclization through SnoopLigation [48, 49] instead of SICLOPPS. SnoopTag and SnoopCatcher form a covalent bond based on SnoopLigation, fully orthogonal to SpyLigation, which permits full decoupling of logic configuration and material crosslinking [50]. SnoopTag was installed on the N-terminus, followed by two protease cleavage sequences flanking mGL and SnoopCatcher, allowing for internal cyclization, followed by the third cleavage sequence, creating a bespoke branched structure. (6) The OR-OR gated construct [i.e., A∨T∨C] was designed with three protease substrate sequences expressed directly in series. (7) The AND-AND construct [i.e., A∧C∧T] relies on two

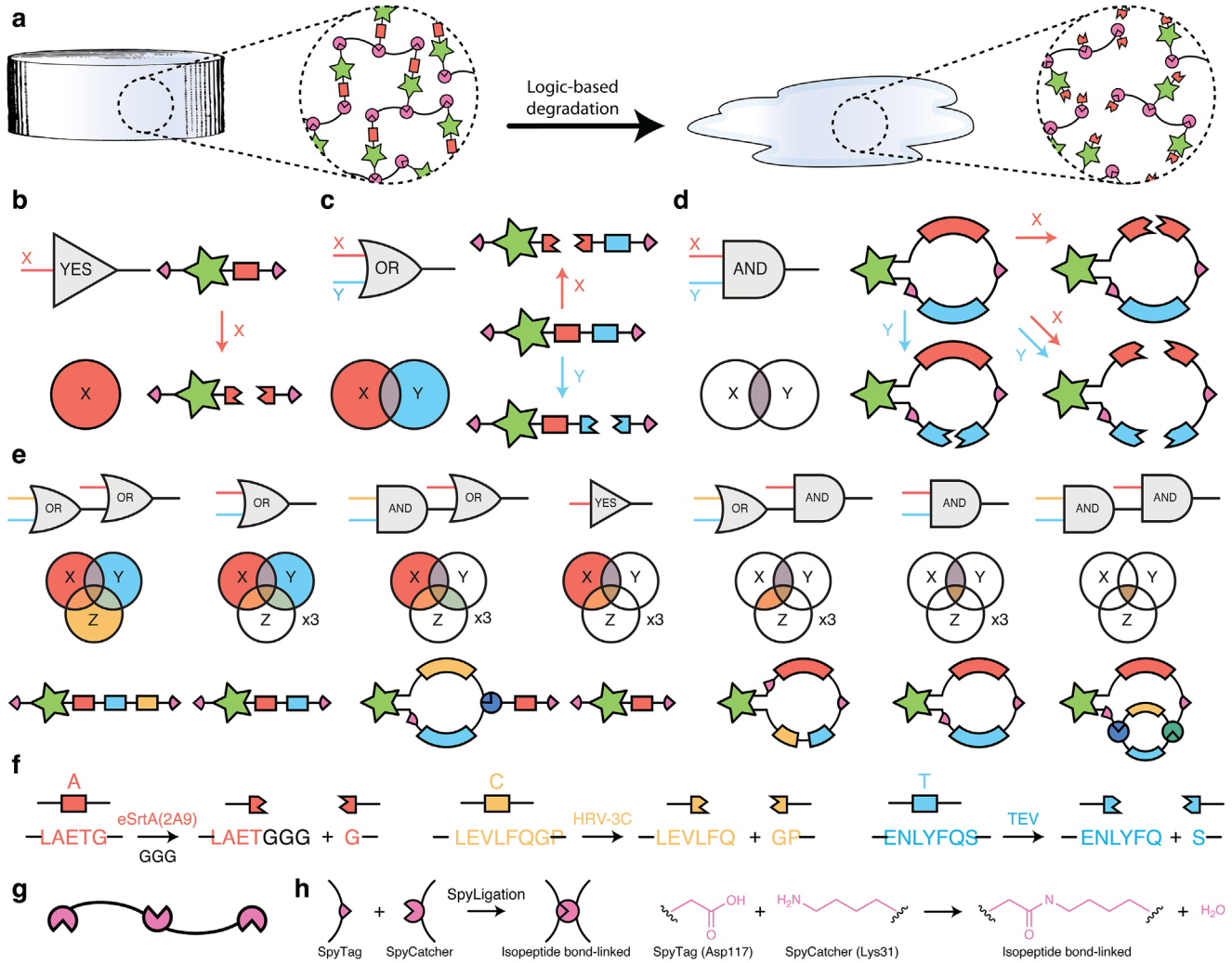

FIGURE 1 | Autonomous compilation of Boolean-responsive protein biomaterials. (a) Covalently crosslinked recombinant protein hydrogels degrade following Boolean logic in response to user-specified inputs. In this example, material dissolution follows YES-gated logic. (b) Single-input YES gate, where in the presence of the correct input, the peptide backbone is cleaved, degrading the crosslink. The green star represents the cargo, colored square represents a protease cleavage site, and the pink triangle represents SpyTag. (c) Dual-input OR gate, formed by two inputs in series. Only one input needs to be present to degrade the material. (d) AND gate, two inputs organized in parallel, where both inputs are required for dissolution. (e) All possible nested logical operators, flanked by SpyTags for material creation. Venn diagrams represent unique combinations of protease inputs and whether the crosslink is predicted to cleave (colored) or remain intact (white). (f) Orthogonal protease actuators are utilized as logical inputs. eSrtA(2A9) degrades LAET↓G (denoted as A), HRV-3C cleaves LEVLFQ↓GP (referred to as C), and TEV acts upon ENLYFQ↓S (denoted as T). (g,h) Crosslinks undergo covalent step polymerization with an elastin-like polypeptide containing three SpyCatchers via SpyLigation. Adapted with permission [34]. Copyright 2025, Nature. Adapted with permission [35]. Copyright 2025, Wiley-VCH GmbH.

orthogonal Tag/Catcher ligations occurring in tandem to form a bicyclic protein cargo. Here, SnoopTag is installed at the cargo's N-terminus and a DogTag [39] at the C-terminus, with their cognate Catchers located internally within the expression frame.

Plasmids encoding all 17 possible logical operators were transformed into BL21(DE3) *Escherichia coli (E. Coli)*, then expressed utilizing standard protocols (Supporting Information). Following cell lysis, proteins were purified by IMAC; cyclic constructs were further purified via size exclusion chromatography (SEC) to separate the target monocyclical constructs from higher-order macrocycle by-products that can result from SICLOPPS, SnoopLigation, and DogLigation (estimated to be ~25%, per SEC analysis, Supporting Information). Protein constructs were characterized and assessed for purity via liquid chromatography-mass spectrometry (LC-MS). All constructs were acquired in high purity and good yield, achieving between 20 mg L^{-1} and 40 mg L^{-1} of culture (Figure S2). Owing to the efficient autonomous compilation of logical gates and reliance on technologies already used in bioprocessing, we anticipate that the synthesis of such crosslinks could be readily scaled for true therapeutic deployment.

The bulk material network was assembled from elastin-like polypeptides with three bisecting SpyCatchers (denoted ELP-TriCatcher, Figure 1g). ELPs are intrinsically disordered engineered protein polymers that are derived from elastin, a commonly occurring extracellular matrix protein [51]. ELPs have found routine use as material backbones due to their ease of

expression, nonimmunogenicity, and elastic properties [23, 25, 52–54]. ELP-TriCatcher was expressed and purified in a similar manner in high purity and yield (50 mg L^{-1} of culture) (Figures S2 and S3). Upon mixing of SpyTag-containing crosslinks and ELP-TriCatcher in a 1:1 stoichiometric ratio of Tag:Catcher motifs, the hydrogel forms via covalent step-growth polymerization (Figure 1h).

2.2 | Boolean Logic-Based Material Characterization

We first sought to create Boolean logic-responsive protein hydrogels via SpyLigation, then demonstrate their responsiveness to each of the potential protease input combinations. To assemble hydrogels, purified crosslinks and ELP were separately dialyzed in deionized water and aliquoted such that the calculated protein mass could form a 10% weight per volume (w/v) material with a 3:2 molar ratio of crosslinks to ELP-TriCatcher to account for differing numbers of Spy motifs per protein (Supporting Information). The material was then lyophilized separately and resuspended with 10x phosphate-buffered saline (PBS) at half the total hydrogel volume. Upon mixing, we observed the rapid formation of a distinct hydrogel.

We then engineered hydrogels with all 17 crosslinks to demonstrate their ability to degrade and release their mGL cargo in response to specific combinations of protease actuators. Materials were subjected to all possible protease input combinations involving eSrtA(2A9), HRV-3C, and TEV (inputs denoted $_A$, $_C$, and $_T$, respectively; $_N$ indicates no protease) then incubated for four hours at 37°C in a shaker incubator (Supporting Information). Supernatant was then collected and its fluorescence measured on a plate reader to determine the percentage of material degradation and mGL cargo released (Figure 2a). As expected, the hydrogels degraded according to their associated logical operation with high specificity (Figure 2b–h; Figure S4). Excitingly, these materials exhibited negligible off-target release, significantly less than our previously reported synthetic polymer-based logic responsive materials, attributed to high protein crosslinker purity and sequence specificity for the protease actuators deployed [32]. The scalability of inputs for these materials is governed by the availability of orthogonal proteases and stimuli-responsive protein-cleavage mechanisms. Prior work from our group has demonstrated systems responsive to up to five inputs [34], as well as both protease- and light-responsive topologies [35], highlighting the extensibility of this design strategy that could be applied to future crosslinks. Due to the inherent binary nature of the output, degradation kinetics are controlled by the rate-limiting protease, where enzyme concentration, temperature, and pH can serve as variables to tune activity [34]; these variables can limit the use of exogenous proteases in vivo, resulting in reduced activity or inactivation, as well as off-target cleavage from environmental proteases [55, 56]. If endogenous proteases are utilized as inputs, orthogonality must be rigorously tested to ensure proper logic operation. Alternatively, temporal control can be user-programmed based on selected logic gates such that degradation is reliant on the timing of protease introduction from the user or the environment. These results demonstrate for the first time the ability to encode biocomputation within genetically encoded materials in a modular fashion.

We next sought to determine the mechanical properties of our Boolean logic-responsive materials via in situ rheological analysis. mGL-A∨T and ELP-TriCatcher were resuspended individually at proper concentration, briefly mixed, then loaded on a rheometer with parallel-plate geometry (8 mm plate diameter, 500 μm gap). Informed by the frequency sweep and shear strain sweep, 1% shear strain and 1 Hz were chosen as rheological parameters, as these were both within the linear viscoelastic range (LVER) of the biomaterial (Figure S5a,b). A time sweep (1% shear strain, 1 Hz) was performed at 25°C and 37°C in triplicate to determine the material stiffness. Material stiffness did not vary between tested temperatures, with storage moduli of 400 ± 43 Pa (25°C) and 426 ± 50 Pa (37°C) (Figure S5c,d). Further, we explored the impact of protease actuators on material viscoelastic properties. The crosslink mGL-(A∧T)∨C was pretreated with all possible input combinations for three hours at 37°C, then the sample viscoelasticity was rheologically assessed following stochiometric reaction with the ELP-TriCatcher (Figure S5e,f). Gel formation occurred rapidly for materials with fully or partially intact crosslinks (e.g., $_N$, $_A$, and $_T$ treatments), while all other conditions did not yield gelation as expected following their programmed logical operation, corroborating observations in the aforementioned in vitro gel degradation studies.

2.3 | Controlled Release of Therapeutics Following Boolean Logic

Heartened by the ability to control material degradation with precise specificity, we next sought to demonstrate controlled release of bioactive protein therapeutics. By exchanging mGL for a therapeutic protein, we can create a prodrug-like material – a "drugamer" – that utilizes biocomputation to dictate release in response to environmental cues. We chose to incorporate recombinant human epidermal growth factor (EGF), which is commonly administered to aid wound healing as it promotes angiogenesis, cellular proliferation, and extracellular matrix remodeling [57, 58]. We swapped mGL for EGF in the A∨C and (A∧T)∨C crosslinks, then expressed and purified these proteins following traditional methods with endotoxin removal (Figure S6). Due to the potency of EGF, final materials were formulated whereby 10% of the crosslinks featured EGF and the other 90% contained a non-bioactive maltose-binding protein (MBP) with the same logical responsiveness (Figure 3a). Therefore, the A∧C-gated materials were calculated to contain 30 μg of the EGF-containing crosslink, while the (A∧T)∨C-gated materials contained 50 μg. Materials (10 μL, 10% w/v) were prepared as previously mentioned, creating drugamers that release the payload upon bulk degradation. The hydrogels were treated with all possible protease input combinations, then incubated at 37°C for two hours until full dissolution. Supernatant was collected and then frozen until analysis.

To determine EGF release from materials and assess bioactivity, we used a human embryonic kidney (HEK293T) reporter cell line that expresses firefly luciferase in response to the Serum Response Element (SRE) [35] (Figure 3b). When EGF is added to SRE HEKs, the SRE genetic element is activated, resulting in cells that luminesce in the presence of luciferin. We first tested if unbound and intact crosslinks (EGF and MBP for each logic response) are bioactive, utilizing commercially purchased recombinant human

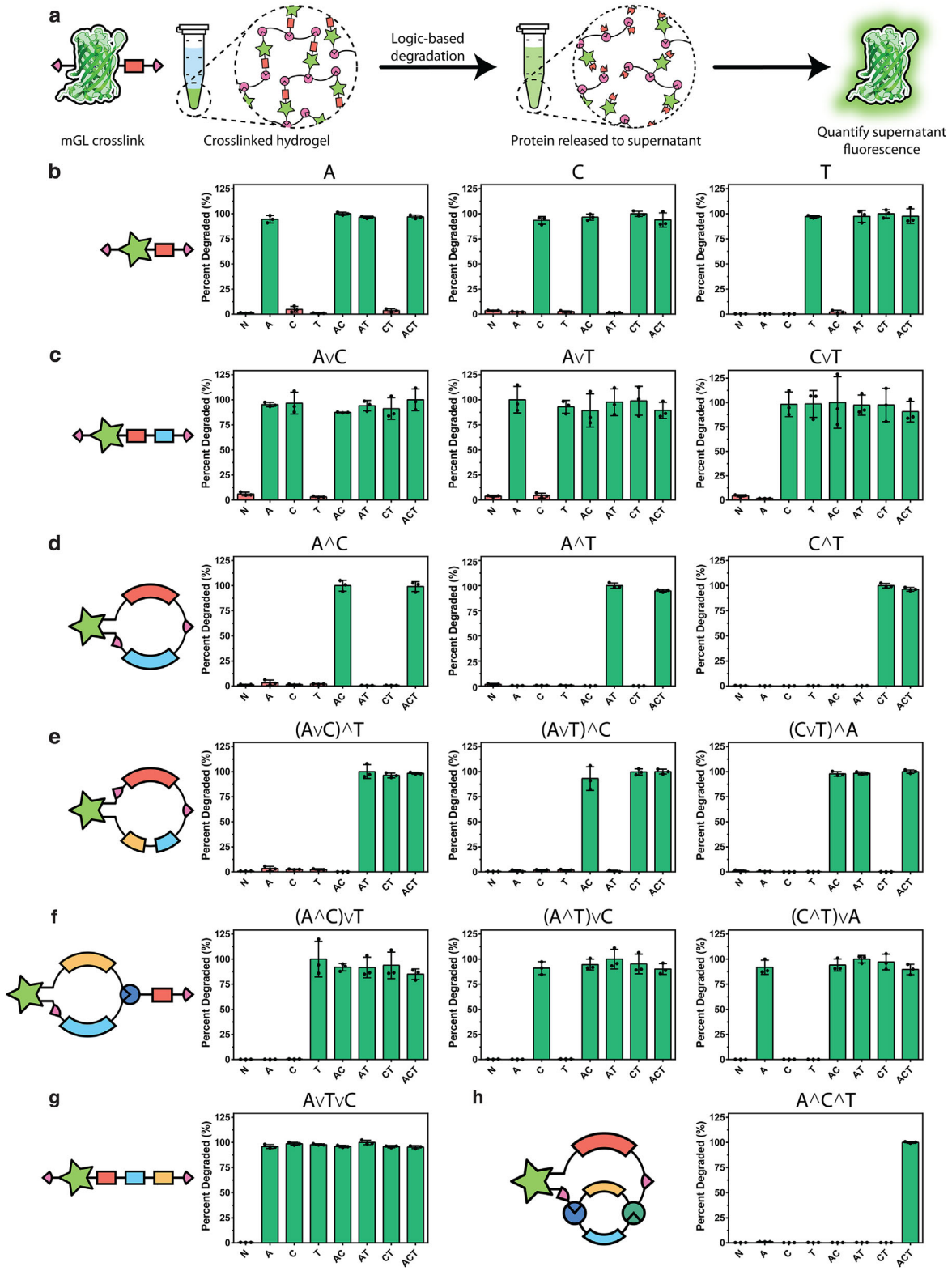

FIGURE 2 | Protein hydrogel degradation and mGL cargo release via protease actuators. (a) Logic-degradable protein hydrogels were subjected to all possible protease input combinations. As materials degrade, mGL payload was released into the supernatant, allowing for fluorescence quantification of material degradation. (b) The response profiles of YES-gated single-input materials. (c, d) The response profiles of the two-input (c) OR-gated and (d) AND-gated constructs. (e–h) The response profiles of the three-input (e) (OR)AND-, (f) (AND)OR-, (g) OR-OR-, and (h) AND-AND-gated systems. Plot titles correspond to the protein crosslink identity; the y-axis represents percent of material degraded as measured through supernatant fluorescence; the x-axis indicates treatment conditions, wherein $_N$ indicates no treatment, $_A$ indicates eSrtA(2A9), $_C$ indicates HRV-3C, and $_T$ indicates TEV. Bars for conditions in which release is expected are colored green, while those unexpected are colored red. Error bars correspond to ±1 standard deviation about the mean for N = 3 replicates.

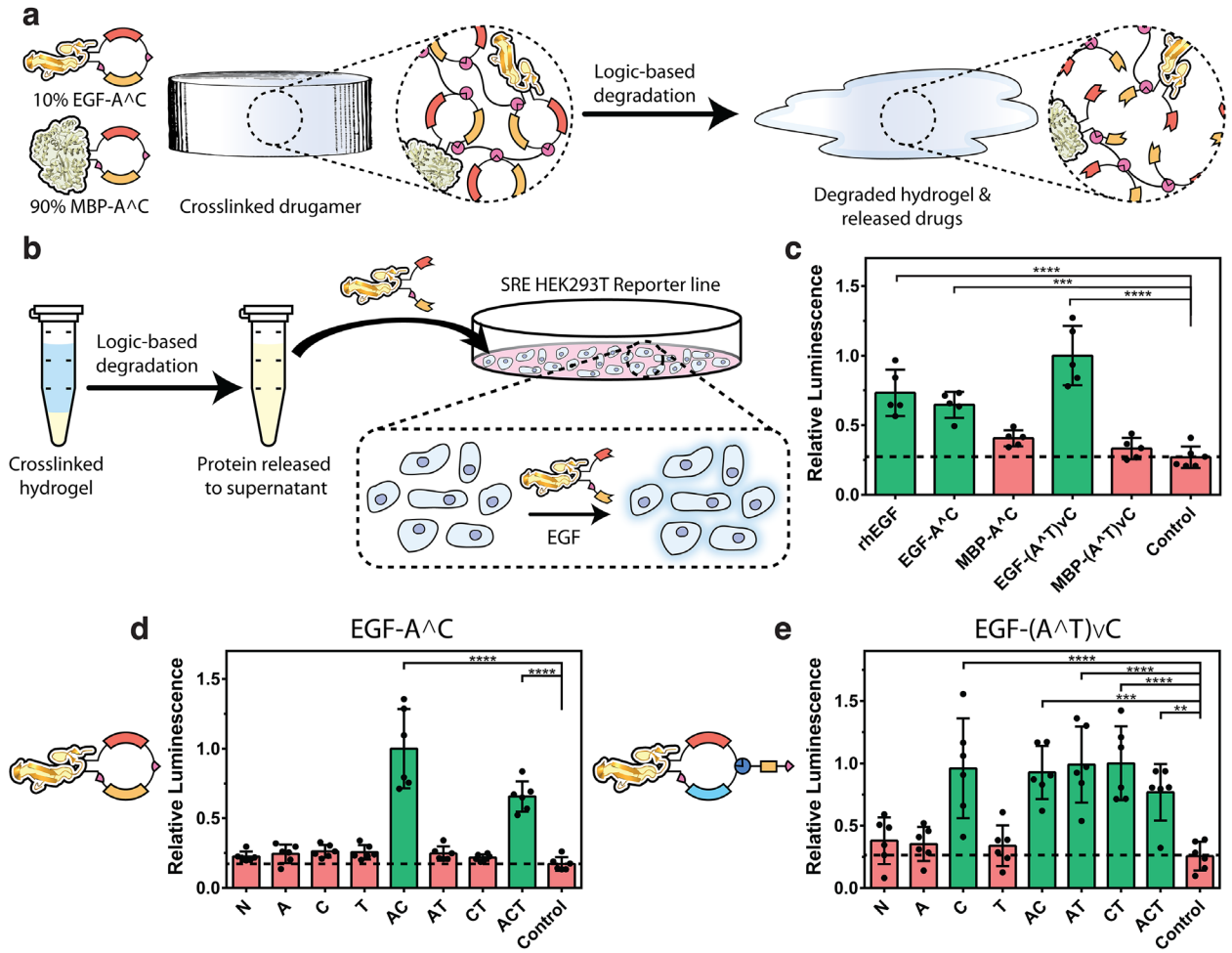

FIGURE 3 | Logic-dictated release of bioactive EGF from Boolean logic-gated materials. (a) Protein drugamer materials were formed with 10% EGF- and 90% MBP-containing crosslinks. In this example, EGF and MBP are genetically incorporated within A∧C. Upon gated degradation, the materials release monomeric MBP and bioactive EGF. (b) To assess EGF release and bioactivity, supernatant was tested by a SRE HEK293T reporter cell line that expresses luciferase upon activation of SRE by EGF. (c) Bioactivity of EGF and MBP crosslinks in solution before protease treatment compared to commercially purchased recombinant human (rh)EGF. EGF-containing crosslinks exhibit similar activity to the commercial rhEGF, while MBP is not significantly different than the untreated control. (Crosslinks, N = 5. Control, N = 6). (d,e) Detection of EGF in supernatant post-protease treatment for (d) A∧C- and (e) (A∧T)∨C-gated materials, N = 6. Bars for expected release are colored green, while unexpected releases are red. $_N$ indicates no treatment, $_A$ indicates eSrtA(2A9), $_C$ indicates HRV-3C, and $_T$ indicates TEV. Error bars correspond to ±1 standard deviation about the mean. Data points that fell outside the interquartile range were determined to be outliers and were excluded. One-way ANOVA test with Dunnett's Post-Hoc analysis comparing each condition to the control, $\alpha = 0.05$. ** = $p < 0.005$, *** = $p < 0.0005$, **** = $p < 0.0001$. Unless marked, all other conditions are not significant.

(rh)EGF and untreated samples as control groups. Upon addition of the crosslinks [i.e., EGF-A∨C, MBP-A∨C, EGF-(A∧T)∨C, MBP-(A∧T)∨C], only EGF-containing crosslinks exhibited bioactivity similar to commercial rhEGF, while MBP crosslinks did not elicit a cellular response above the baseline SRE activation seen in the untreated reporter cells (Figure 3c). Genetic fusion of logical operators with therapeutic cargo and cyclization did not interfere with bioactivity as previously seen [35], but interestingly, the SICLOPPS-mediated AND-gate had slightly reduced activity compared to the SnoopLigation (AND)OR gate, potentially due to increased cyclic strain. Although EGF bioactivity is retained within the crosslinker, its covalent immobilization within the hydrogel network is expected to limit receptor interactions prior to protease-triggered release, reducing the likelihood of premature signaling in surrounding cells if applied in vivo [59, 60]. Supernatant from the protease-degraded A∧C- and (A∧T)∨C-gated materials was then added to the SRE HEKs. As programmed, only conditions that were expected to degrade and yield release exhibited bioactivity with little off-target release compared to the control (Figure 3d,e). This approach affords precise control over therapeutic release, demonstrating what we believe to be the first report of a recombinant protein-based drugamer while opening doors for future controlled delivery applications.

2.4 | Release of Cells from Materials Following Boolean Logic

The delivery of therapeutic cells holds promise due to their ability to sense environmental stimuli and dynamically respond, allowing for therapeutic action on previously intractable diseases [61]. Unfortunately, cell-based therapies often struggle with reduced cellular survival, loss of phenotype, and off-target

effects post-transplantation [61, 62]. By encapsulating cells within biomaterials and only releasing them site-specifically, we could potentially increase the survival of cellular therapeutics [61, 63]. The utilization of a multi-stimuli responsive biomaterial would enable release only when multiple disease biomarkers are present, thereby improving specificity.

First, we verified that cells can be readily encapsulated within our gels in a cytocompatible manner. Fibroblast-like HS-5 cells were entrapped in a non-fluorescent MBP-A∨T∨C gel, incubated for 24 h in traditional cell culture conditions, and then assayed for viability (Calcein AM live stain, Hoechst 33342 nuclear stain) (Supporting Information). Cell-laden gels incubated in 50% DMSO overnight served as dead controls. Stained cells were then imaged on a Leica Stellaris 5 confocal microscope (Leica, Wetzlar, Germany; Leica Application Suite X 4.5.0.25531), where cells that double-stained for Calcein AM and Hoechst 33342 were considered alive, while those that only stained with Hoechst 33342 were dead (Figure S7). The encapsulated cells exhibited 90.7% ± 5.5% viability, demonstrating that the materials are not cytotoxic regardless of covalent crosslinking via SpyLigation and encapsulation after 24 h.

We next sought to release cells from three different logic operations, allowing for multiplexed cell release. We individually encapsulated three cell lines that express spectrally separate fluorescent proteins within each uniquely crosslinked material to mimic therapeutic release (Figure 4a). We utilized mGL-A∨C crosslinks to encapsulate HS-5 mTag blue fluorescent protein (BFP)-expressing cells, mGL-YES-T hydrogels to release HS-5 red fluorescent protein mCherry$^+$ cells, and mGL-(C∧T)∨A materials were used to encapsulate HEK293T stably expressing an enhanced monomeric infrared fluorescent protein (emiRFP) that excites at 703 nm [64]. HS-5 mTagBFP$^+$ cells and HS-5 mCherry$^+$ cells were used in prior studies [32], while HEK293T emiRFP$^+$ cells were newly generated for these studies via lentiviral transfection (Figure S8). Upon encapsulation, hydrogels were treated with all 8 possible protease combinations; flow cytometry was then used to determine fluorescent composition of the released cell populations (Figures S9 and S10). When compared to expected response profiles (Figure 4b), materials released cells according to their logical operation, demonstrating tight control over cell presentation (Figure 4c; Table S1). We attribute the low levels of off-target release (measured at <8%) to cell escape from the material edges during supernatant collection. As several prior studies have shown no inflammatory responses from materials containing ELPs [21, 52, 54, 65, 66] or protein click-like chemistries [16, 21, 52, 66], we anticipate that these materials and their degraded byproducts would be nonimmunogenic in an in vivo setting. Based on protease treatment, these materials can be utilized for multiplexed – and/or potentially sequential – cell release, highlighting their applicability for tissue engineering and therapeutic delivery.

3 | Conclusion

In this manuscript, we engineered the first fully recombinant protein-based materials whose bulk degradation and bioactive cargo release can be specified through Boolean logic. With the addition of three orthogonal proteases, degradation is tightly controlled, with minimal off-target cargo release. By employing genetically encoded materials, protease-recognition sequences, and therapeutic cargo(s), response to user-specified disease signatures can be readily encoded. For instance, materials sensitive to proteases upregulated during wound healing could control the release of EGF to coincide with a desired healing stage, while exogenous proteases could be co-delivered to provide user control. Furthermore, we demonstrated the applicability of these multi-stimuli-responsive materials for controlled delivery by dictating the release of both protein and cell therapies. We anticipate that these materials could unlock a new suite of applications across drug delivery, tissue engineering, and biosensing.

4 | Experimental Section

4.1 | General Method for Protein Expression

E. Coli BL21.(DE3) (NEB) were transformed with plasmids, then expressed using routine protein expression protocols. In short, bacteria were grown in Luria-Bertani (LB) media [tryptone 1% (v/w), yeast extract 0.5% (v/w), 85.56 mM NaCl, pH 7.0] with kanamycin (30 μg mL^{-1}) at 37°C in a shaker incubator (220 rpm) until an optical density (OD) of 0.4–0.6 was reached. Isopropyl β-D-1-thiogalactopyranoside (IPTG) was then added to induce protein expression. If constructs are linear, 0.5 mM of IPTG was used; otherwise, cyclic constructs were induced with 0.4 mM. The cultures were then moved to a reduced temperature (16°C) for 18 h. Cells were harvested via centrifugation (4,000 g, 20 min, 4°C) and stored at −80°C until use.

4.2 | Protein Purification via Immobilized Metal Affinity Chromatography (IMAC)

Cell pellets were reconstituted in 40 mL of lysis buffer (20 mM Tris, 50 mM NaCl, pH 7.5). These were then supplemented with phenylmethylsulfonyl fluoride (PMSF) to a final concentration of 1 mM and sonicated on ice (18 min at 30% amplitude and 33% duty cycle) (Fisher Scientific; Waltham, MA). After sonication, the cell lysate was centrifuged for 45 min at 11,000 g to separate soluble from insoluble fractions.

Clarified lysate was loaded onto an ÄKTA Pure 25L FPLC (Cytiva; Marlborough, MA) equipped with a 5 mL HisTrap HP column at a flow rate of 5 mL/min. The HisTrap column was first equilibrated with 5 column volumes (CV) of lysis buffer prior to loading. Once all protein was bound, the column was washed with 10+ CVs of lysis buffer until residual UV read-outs (λ = 280 nm) dropped to 0 absolute units (au). The target protein was then eluted from the column into a 96-well plate by switching to elution buffer (lysis buffer supplemented with 250 mM imidazole). Elution fractions were assessed for purity by preliminary sodium dodecyl-sulfate polyacrylamide gel electrophoresis (SDS-PAGE); the purest fractions were then pooled pending further dialysis or SEC.

For SDS-PAGE, samples were mixed with 2x Laemmli sample loading buffer (125 mM Tris base, 4% SDS, 20% glycerol, 0.01% Bromphenol blue, 10% β-mercaptoethanol) and boiled at 99°C for 10 min. Samples were loaded into precast 8–16% miniProtean

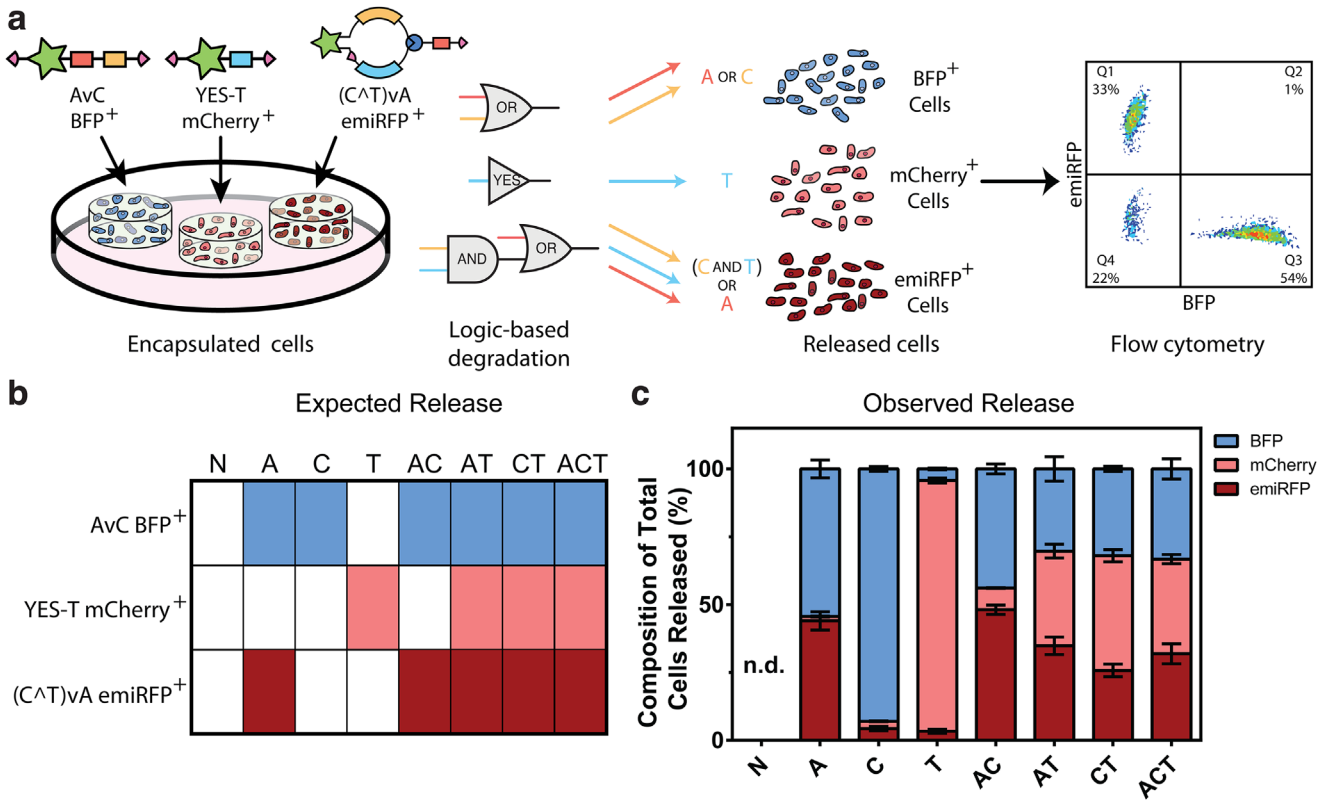

FIGURE 4 | Release of entrapped fluorescent cells from logically responsive recombinant protein materials. (a) mGL-A∨C hydrogels were employed to release encapsulated HS-5 BFP2$^+$ cells, mGL-YES-T hydrogels contained HS-5 mCherry$^+$ cells, and mGL-(C∧T)∨A materials mediated HEK293T emiRFP703$^+$ cell release. Materials were treated with all possible input protease combinations, resulting in material dissolution and accompanying cell release according to their programmed Boolean operations. Released cell population compositions were measured by flow cytometry. (b) Expected degradation and fluorescent cell release, where colored boxes correspond to expected release per protease treatment. (c) Observed cell release following protease treatment. Stacked bars correspond to the mean per cell population, where error bars (±1 standard deviation) are displayed on top of each cell population bar. N = 3.

gel (BioRad) in tris-glycine running buffer (25.0 mM Tris base, 192.4 mM Glycine, 3.5 mM SDS), then run at 130 V. The miniProtean gels were stained with Coomassie Blue dye, following standard staining protocol (stain: 0.1% Coomassie Blue R250, 30% methanol, 5% acetic acid, destain: 30% methanol, 5% acetic acid) and imaged with true color on an Azure 600 AZI600 scanner.

For linear constructs that had no higher-order macro-cycle contaminants, the pooled purified protein was dialyzed (20 mM Tris, 50 mM NaCl, pH 7.5) to remove imidazole (SnakeSkin Dialysis Tubing, 10K MWCO. Fischer Scientific; Waltham, MA). After 4+ dialysis bath changes, proteins were spin-concentrated if needed using an Amicon Ultra 15 centrifugation filter (10 kDa cutoff. Sigma-Alrich; Burlington, MA) to reach a concentration between 2 mg mL^{-1} and 2.5 mg mL^{-1}. The purified solution was supplemented with glycerol (10% of the final volume) to act as a cryoprotectant, aliquoted into single-use tubes to avoid repeated freeze-thaw cycles, and flash-frozen with liquid nitrogen prior to long-term storage.

4.3 | Size-Exclusion Chromatography (SEC)

For cyclized constructs, proteins were loaded again onto an ÄKTA Pure unit equipped with a HiLoad 26/600 Superdex 75pg SEC column. The column was equilibrated with a high-salt buffer solution (20 mM Tris, 300 mM NaCl, pH = 7.5). Sample injection occurred at a flow rate of 2.6 mL/min. Buffer flow rate through the system occurred at 1.5-1.8 mL/min, depending on the purity of the injected solution. Purified eluates were collected in 96-well plates. Prior to pooling, preliminary SDS-PAGE was conducted to verify fraction purity. Proteins were then spin-concentrated using an Amicon Ultra 15 centrifugation filter (10 kDa cutoff, Sigma-Aldrich; Burlington, MA) and then stocked as described in Method 4.2.

4.4 | Liquid Chromatography-Mass Spectrometry (LC-MS)

Protein identity and purity were confirmed through LC-MS. Each sample was filtered (0.22 μm), then injected into an LC-MS (AB-Sciex 5600 QTOF) using an inline polymeric reversed-phase column (PL 1912-1503, Agilent). Protein solutions were separated over the following 15 min linear gradient: 10% acetonitrile (ACN) for 5 min, then linear gradient from 10% to 90% ACN over 10 min, with mass spectrum scans taken every 1 s in positive mode. The chromatogram was integrated, and the full molecular weight was calculated using Analyst (AB Sciex).

4.5 | Hydrogel Creation

To formulate hydrogels, previously stocked logical operators and ELP-TriCatcher were thawed on ice and dialyzed in deionized (DI) water at 4°C (SnakeSkin Dialysis Tubing, 10K MWCO). All constructs except for linear logical operators (YES/OR) were dialyzed for 2 h with one volume change after an hour. Linear constructs were dialyzed for 1 h to 1.5 h and carefully watched to ensure no protein crashed out of solution. Protein concentration was determined via NanoDrop microvolume spectrophotometer and aliquoted based on the mass of protein needed to make a 10% weight/volume (w/v) hydrogel. An Excel sheet was utilized to calculate the ratio of crosslink and ELP-TriCatcher needed to make a predetermined hydrogel volume, taking into account each construct's molecular weight and number of Spy chemistry motifs. Proteins were then flash frozen and lyophilized overnight, keeping crosslinks and ELP-TriCatchers separate until the point of material creation. Material was resuspended with 10x phosphate-buffered saline (PBS) with half the hydrogel volume (i.e., if creating a 10 µL gel, resuspend crosslinks in 5 µL and ELP-Tricatcher in 5 µL), then incubated at 37°C for 20 min. ELP-TriCatcher was vigorously stirred with a pipette tip and briefly centrifuged until completely resuspended. Crosslinks and ELP-TriCatcher were then combined, quickly mixed with a pipette tip, and centrifuged to remove bubbles. Materials were incubated at 37°C for two hours to solidify into hydrogels.

4.6 | Material Degradation via Protease Actuators

Each construct was created into 10 µL hydrogels (see Method 4.5) for all possible combinations of protease actuators ($_A$, $_C$, $_T$) in triplicate (8 inputs x 3 per crosslink type). Reaction buffer was prepared (final concentration: 5 mM of DTT, 5 mM of $CaCl_2$, 1x triglycine, proteases at 2uM, 20 mM Tris, 50 mM NaCl, pH 7.5) and 200 µL was added to each hydrogel. Images were immediately taken (T = 0 h) with an iPhone camera, then materials were incubated at 37°C on a shaker incubator with slight agitation (100 rpm) for up to 4 h. Images were then retaken at hour 4 (T = 4 h), and the supernatant was sampled. Material supernatant was added to a black-walled 96-well plate, then fluorescence was read on a BioTek Synergy Microplate Reader (BioTek, Winooski, VT; Gen5 v3.09 software). Fluorescence measurements, calculated in Microsoft Excel, were normalized by calculating the average fluorescence per input, assuming the condition with the brightest fluorescence average was 100% released (visually verified from gel degradation images in Figure S4). The normalized percentage of cargo released for all collected replicates was then calculated relative to the determined fluorescence measurement for 100% released.

4.7 | Rheological Analysis of Material Viscoelasticity

Rheological analysis was performed on an Anton Paar Physica MCR 301 Rheometer with parallel-plate geometry (8 mm plate diameter, 500 µm gap). Plate temperature was controlled via a circulating water bath. The crosslink A∨T was created into a 30 µL hydrogel (see Method 4.5), then incubated on the rheometer for 1 h at room temperature. To determine the material linear viscoelastic range, an angular frequency sweep (1% shear strain, 0.1 Hz to 10 Hz) and strain sweep (0.1% to 100% shear strain, 1 Hz) were performed in triplicate at 37°C. Then, a time sweep (1% shear strain, 1 Hz) at 25°C and 37°C was performed to assess material stiffness in triplicate.

The crosslink (A∧T)∨C was resuspended to create 30 µL hydrogels with protease treatment buffer (final concentration: 5 mM of DTT, 5 mM of $CaCl_2$, 1x triglycine, proteases at 2 uM, 20 mM Tris, 50 mM NaCl, pH 7.5) for all possible input combinations for three hours at 37 C. The rheometer was pre-heated to 37°C via a water bath. Crosslinks and ELP-TriCatcher were mixed, then pipetted onto the rheometer parallel plate. A time sweep (1% shear strain, 1 Hz) was immediately started to capture gel formation over 300 s.

4.8 | Expression and Purification of EGF and MBP Crosslinks

Plasmids for SpyTag-EGF-A∧C-SpyTag and SpyTag-EGF-(A∧T)∨C-SpyTag were transformed into SHuffle T7 Competent E. coli (NEB, C3029J), while the plasmids for SpyTag-MBP-A∧C-SpyTag, SpyTag-MBP-(A∧T)∨C-SpyTag, and SpyTag-MBP-A∨T∨C-SpyTag were transformed into BL21(DE3) E. Coli (NEB). Proteins were expressed with standard protocol, except the EGF constructs in Shuffle cells were incubated at 30°C in LB media until an OD of 0.4-0.5. IPTG (0.4 mM) was added to induce protein expression and incubated overnight at 16°C. Standard purification with an endotoxin wash (standard lysis buffer supplemented with 0.1% triton X-114) and dialysis protocols were followed.

4.9 | EGF Release from Hydrogels

Hydrogels (10 µL, 10% w/v) were formed as described in Method 4.5, where 90% of the crosslinks contained Maltose Binding Protein (MBP) cargo and the remaining 10% contained Epidermal Growth Factor (EGF). This resulted in the A∧C-gated materials containing 30 µg of EGF, while the (A∧T)∨C-gated materials contained 50 µg of EGF. Materials were incubated for 2 h at 37°C, then washed two times with buffer (20 mM Tris, 50 mM NaCl, pH 7.5) for 1 h each at 37°C. All possible combinations of endotoxin-free proteases were then added in reaction buffer (final concentration: 3 mM of DTT, 3 mM of $CaCl_2$, 1x triglycine, 20 mM Tris, 50 mM NaCl, pH 7.5), where $_A$ was added at 2 µM, $_C$ was added at 4 µM, and $_T$ was added at 3 µM. Materials were incubated for 2 h at 37°C until fully dissolved. Supernatant was sampled for the EGF bioactivity assay to detect the presence of released EGF.

4.10 | EGF Bioactivity Assay

EGF bioactivity was determined using a Human embryonic kidney (HEK293T) (ATCC, CRL-3216) Serum Response Element (SRE) Luciferase reporter cell line, created in previously reported work [35]. Briefly, HEK293T cells were transfected with SRE Luciferase Reporter Lentivirus (78627, BPS Bioscience) and selected with Puromycin to generate a stable cell line.

SRE cells were seeded at 1.5×10^3 cells in a clear-bottom white-walled 96-well plate in Dulbecco's Modified Eagle Medium (DMEM) supplemented with 10% fetal bovine serum (FBS) and 1% penicillin-streptomycin (P/S). The following day, the media was removed, and the cells were washed once with PBS, then serum-free cell culture media was added (DMEM, 1% P/S). The next day, commercial rhEGF (R&D Systems, 236-EG-200), EGF crosslinks, and MBP crosslinks were added to the cells at 200 ng mL^{-1}. Alternatively, collected supernatant from protease-treated EGF gels was added to the cells at 200 ng mL^{-1}. Cells were then left to incubate at 37°C, 5% CO_2 with saturating humidity for 6 h. CellTiter-Fluor Cell Viability Assay (G6080, Promega) was mixed in a 1:5 ratio with the cell media as directed by the manufacturer's instructions. The plate was incubated at 37°C for 30 min, then fluorescence was read on a plate reader. One-GLO Luciferase Assay (E6110, Promega) was then added to the cells according to manufacturer instructions, and the plate was incubated for 5 min at room temperature on a shaker, then luminescence was read on a plate reader. Relative luminescence was calculated by finding the ratio between luminescence and fluorescence to normalize to the cell count, then averaging the ratios per input condition, where the largest average was designated the maximum. Ratio of each replicate luminescence to the maximum was then determined. The data was checked for outliers by analyzing the interquartile range, and any outliers were removed from the analysis.

4.11 | Cytocompatibility Testing

Hydrogels (10 µL, 10% w/v) were formed as described in Method 4.5 with MBP-A∨T∨C to encapsulate cells. To encapsulate cells, the crosslink was co-resuspended with HS-5 cells (ATCC CRL-3611) at 3.0×10^6 mL^{-1} before mixing with the ELP TriCatcher. The gels were plated on a non-tissue-treated glass-bottom dish. The encapsulated cells were then incubated in DMEM supplemented with 10% FBS and 1% P/S for 24 h at 37°C, 5% CO_2 with saturating humidity. Encapsulated dead controls were incubated with 50% dimethyl sulfoxide (DMSO) in addition to the media. The gels were then stained with 1 µM Calcein AM and 1:1000 Hoechst 33342 for 1 h at 37°C. Gels were then imaged on a Leica Stellaris 5 confocal microscope (Leica, Wetzlar, Germany; Leica Application Suite X 4.5.0.25531) at 10x magnification. ImageJ 1.53c was used to process the images and count the number of alive cells and nuclei. 13 gel regions in 3 "Encapsulated" gels were analyzed (N = 1831 cells), while 8 gel regions in 3 "Encapsulated + 50% DMSO" gels were analyzed (N = 800 cells). Percent live was calculated by dividing the number of double-stained, "Live", cells by the total number of nuclei per image, at which all regions were averaged and standard deviation calculated.

4.12 | Generation of Fluorescent Cell Lines

For our tri-color cell release studies, we used a mTagBlue fluorescent protein (BFP) expressing HS-5 cell line and a mCherry expressing HS-5 cell line used in prior research from our lab. We identified enhanced monomeric infrared fluorescent protein (emiRFP) [64] that excites at 703 nm as a third fluorescent protein with minimal cross-talk with BFP and mCherry. A new stable cell line was generated.

To generate a stable cell line, lentivirus was first made. HEK293T cells were plated at ~40% confluency and allowed to adhere to tissue culture plastic overnight. Fresh media was added, then HEKs were transfected with envelope plasmid pMD2.G (Addgene #12259), packaging plasmids pMDLG/pRRE (Addgene #12251) and pRSV-REV (Addgene #12253), and pLenti-emiRFP703 using Lipofectamine 3000 (Invitrogen). Cells were cultured for 2 days post-transfection, and virus-laden media was harvested. Viral media was filtered (0.45 µm) and tested using a lentiviral titration card (ABM Biologics). Once the presence of the virus was confirmed, the virus-laden media was added to fresh HEK293T cells that had been plated at ~40% confluence in a 35 mm dish (Fisher Scientific, Waltham, MA) and had adhered the prior night. The cells were incubated overnight, then the following day, emiRFP production was confirmed via confocal microscopy (Leica, Wetzlar, Germany; Leica Application Suite X 4.5.0.25531). Viral-laden media was removed and bleached to destroy any pendant lentiviral particles. After replenishing the well with fresh DMEM, cells were selected in 6 µg mL^{-1} of Puromycin (Fisher Scientific, Waltham, MA). Cells were incubated in selection media for 24 h, after which non-adherent cells were removed, and fresh DMEM was used to replenish the well, allowing the surviving transgenic cells to recover and expand.

To verify that cells are spectrally separate, BFP^+ HS-5 cells, $mCherry^+$ HS-5 cells, and $emiRFP703^+$ HEK293T cells were seeded on a 4-chamber tissue-treated glass slide (ibidi) in DMEM supplemented with 10% fetal bovine serum FBS and 1% P/S. The following day, the cells were imaged on a Leica Stellaris 5 confocal microscope at 10x magnification. The BFP channel was imaged at an excitation/emission range of 405 nm/425–583 nm, mCherry was imaged at an excitation/emission range of 580 nm/585–690 nm, and emiRFP703 was imaged at an excitation/emission range of 685 nm/690–834 nm. ImageJ 1.53c was used to split imaging channels and add scale bars.

4.13 | Fluorescent Cell Release From Hydrogels

For tricolor cell release, mGL-A∨C hydrogels were used to release HS-5 $mTagBFP2^+$ cells, mGL-T hydrogels were used to release HS-5 $mCherry^+$ cells, and mGL-(T∧C)∨A materials released HEK293T $emiRFP703^+$ cells.

Hydrogel material (10 µL, 10% w/v) was prepped as mentioned in Method 4.5, resuspended in 1x PBS. Lyophilized crosslinks were dissolved, then mixed with the corresponding cells at 10×10^6 mL^{-1}. Crosslink/cell mixtures were mixed with ELP-TriCatcher, then quickly placed in a 24-well plate with non-tissue-treated glass. Gels were incubated for 10 min at 37°C, 5% CO_2 with saturating humidity. Serum-free DMEM was then added, and the gels were incubated for 1 h. The media was then removed to discard any cells that were not encapsulated. Materials were protease-treated as described in Method 4.6 in serum-free DMEM and incubated for 30 min at cell culture conditions. Previous studies have verified that all proteases and buffer components are cytocompatible [34]. Released cells were captured, pelleted (200 x G, 5 min), and washed two times with cold Fluorescence-activated cell sorting (FACS) buffer (PBS, 1% BSA). Population fluorescence was captured on a BD FACS Symphony A3 analyzer (BD Bioscience; San Jose, CA; BD FACSDiva v8.0 software). BFP

was excited with the 405 nm laser and captured with 450 ± 50 nm filters. mCherry was excited with the 561 nm laser and detected with 610 ± 20 nm filters. emiRFP703 was excited with 637 nm laser and detected at 710 ± 50 nm. Data was analyzed in FlowJo v10 to determine the percentage of the population that was positive for BFP, mCherry, and emiRFP703 by histograms, then the data was exported to Excel. Replicates were averaged and standard deviations calculated in GraphPad Prism. Release studies were performed in triplicate.

4.14 | Statistical Analysis

All data was processed and normalized in Microsoft Excel 365. Statistical tests and graphs were completed in GraphPad Prism (version 6). All plots display the mean ± 1 standard deviation about the mean. To normalize data, the average value of all replicates per input was calculated, where the largest average was designated the maximum. The percentage or ratio of each replicate was then calculated relative to the determined maximum. All data presented was performed in varying numbers of replicates of at least $n = 3$ (exact number of replicates marked within each figure caption). To calculate differences in EGF or MBP bioactivity comparing each protease input condition to the control, a One-way ANOVA test with Dunnett's Post-Hoc analysis ($\alpha = 0.05$. ** = $p < 0.005$, *** = $p < 0.0005$, **** = $p < 0.0001$) was used. Outliers were determined using an R script to detect data points that fell outside of the interquartile range (25th–75th percentile) and were excluded from analysis for EGF activity and gel degradation studies.

Author Contributions

Ryan Gharios: conceptualization, data curation, visualization, writing – original draft, writing – review and editing, validation, methodology, investigation. **Shivani Kottantharayil**: data curation, writing – review and editing, methodology, investigation, validation. **Murial L. Ross**: conceptualization, data curation, formal analysis, visualization, writing – original draft, writing – review and editing, funding acquisition, validation, methodology, investigation. **Cole A. Deforest**: conceptualization, funding acquisition, writing – original draft, writing – review and editing, visualization, project administration, supervision, resources.

Acknowledgements

The authors thank J. Davis for gifting HEK293T cells (previously obtained from ATCC, CRL-3216), and J. Hoye for guidance on stable cell line generation. Additionally, the authors gratefully acknowledge Dale Whittington for training and maintenance of the UW Mass Spectrometry Center. This work was supported by a grant (DMR 1807398, C.A.D.) from the National Science Foundation and a Maximizing Investigators' Research Award (R35GM138036, C.A.D.) from the National Institutes of Health. Student support was further provided through the National Science Foundation (DGE-2140004, M.L.R.), Goldwater Scholarship (S.P.K), and a University of Washington Mary Gates Endowment for Students (S.P.K.). Part of this work was conducted with instrumentation provided by the Joint Center for Deployment and Research in Earth Abundant Materials (JCDREAM).

Funding

This work was supported by a grant (DMR 1807398, C.A.D.) from the National Science Foundation and a Maximizing Investigators' Research Award (R35GM138036, C.A.D.) from the National Institutes of Health. Student support was further provided through the National Science Foundation (DGE-2140004, M.L.R.), Goldwater Scholarship (S.P.K), and a University of Washington Mary Gates Endowment for Students (S.P.K.).

Conflicts of Interest

C.A.D., M.L.R., and R.G. have filed a patent application (PCT/US2025/031504) related to the work described in this article. The other authors declare no conflicts of interest.

Data Availability Statement

The data that support the findings of this study are available from the corresponding author upon reasonable request.

References

1. N. E. Gregorio, C. M. Haas, N. P. King, and C. A. DeForest, "Engineering Complexity into Protein-Based Biomaterials for Biomedical Applications," *Nature Reviews Materials* 11 (2025): 328–342, https://doi.org/10.1038/s41578-025-00861-8.

2. S. Hollingshead, C.-Y. Lin, and J. C. Liu, "Designing Smart Materials with Recombinant Proteins," *Macromolecular Bioscience* 17 (2017): 1600554, https://doi.org/10.1002/mabi.201600554.

3. O. S. Fenton, K. N. Olafson, P. S. Pillai, M. J. Mitchell, and R. Langer, "Advances in Biomaterials for Drug Delivery," *Advanced Materials* (2018): 1705328, https://doi.org/10.1002/adma.201705328.

4. N. Davari, N. Bakhtiary, M. Khajehmohammadi, et al., "Protein-Based Hydrogels: Promising Materials for Tissue Engineering," *Polymers* 14 (2022): 986, https://doi.org/10.3390/polym14050986.

5. J. L. Frandsen and H. Ghandehari, "Recombinant Protein-Based Polymers for Advanced Drug Delivery," *Chemical Society Reviews* 41 (2012): 2696–2706, https://doi.org/10.1039/c2cs15303c.

6. K. Z. Lee, J. Jeon, B. Jiang, S. V. Subramani, J. Li, and F. Zhang, "Protein-Based Hydrogels and Their Biomedical Applications," *Molecules* 28 (2023): 4988, https://doi.org/10.3390/molecules28134988.

7. C. Garcia, S. S. Patkar, B. Wang, R. Abouomar, and K. L. Kiick, "Recombinant Protein-based Injectable Materials for Biomedical Applications," *Advanced Drug Delivery Reviews* 193 (2023): 114673, https://doi.org/10.1016/j.addr.2022.114673.

8. A. Varanko, S. Saha, and A. Chilkoti, "Recent Trends in Protein and Peptide-Based Biomaterials for Advanced Drug Delivery," *Advanced Drug Delivery Reviews* 156 (2020): 133–187, https://doi.org/10.1016/j.addr.2020.08.008.

9. J. Zhu and R. E. Marchant, "Design Properties of Hydrogel Tissue-Engineering Scaffolds," *Expert Review of Medical Devices* 8 (2011): 607–626, https://doi.org/10.1586/erd.11.27.

10. M. S. B. Reddy, D. Ponnamma, R. Choudhary, and K. K. Sadasivuni, "A Comparative Review of Natural and Synthetic Biopolymer Composite Scaffolds," *Polymers* 13 (2021): 1105, https://doi.org/10.3390/polym13071105.

11. A. Miserez, J. Yu, and P. Mohammadi, "Protein-Based Biological Materials: Molecular Design and Artificial Production," *Chemical Reviews* 123 (2023): 2049–2111, https://doi.org/10.1021/acs.chemrev.2c00621.

12. G. Xiang, B. Yin, B. Shiroud Heidari, et al., "Programmable Hydrogels: Frontiers in Dynamic Closed-Loop Systems, Biomimetic Synergy, and Clinical Translation," *Advanced Science* 12 (2025): 12037, https://doi.org/10.1002/advs.202512037.

13. R. Gharios, R. M. Francis, and C. A. DeForest, "Chemical and Biological Engineering Strategies to Make and Modify Next-Generation Hydrogel Biomaterials," *Matter* 6 (2023): 4195–4244, https://doi.org/10.1016/j.mtt.2023.10.012.

14. S. Lindsey, J. H. Piatt, P. Worthington, et al., "Beta Hairpin Peptide Hydrogels as an Injectable Solid Vehicle for Neurotrophic Growth Factor

Delivery," *Biomacromolecules* 16 (2015): 2672–2683, https://doi.org/10.1021/acs.biomac.5b00541.

15. B. Jiang, X. Liu, C. Yang, et al., "Injectable, Photoresponsive Hydrogels for Delivering Neuroprotective Proteins Enabled by Metal-directed Protein Assembly," *Science Advances* 6 (2020): abc4824, https://doi.org/10.1126/sciadv.abc4824.

16. J. I. Bennett, M. O. Boit, N. E. Gregorio, et al., "Genetically Encoded XTEN-Based Hydrogels with Tunable Viscoelasticity and Biodegradability for Injectable Cell Therapies," *Advanced Science* 11 (2024): 2301708, https://doi.org/10.1002/advs.202301708.

17. M. L. Ross, S. P. Kottantharayil, T. K. Nguyen, R. Ravichandran, and C. A. DeForest, "Genetically Encoded Interpenetrating Polymer Networks as Injectable Biomaterials for Controlled Therapeutic Protein Delivery," *ACS Biomaterials Science & Engineering* 11 (2025): 4869–4880, https://doi.org/10.1021/acsbiomaterials.5c00813.

18. N. L. Fletcher, C. V. Lockett, and A. F. Dexter, "A pH-responsive Coiled-Coil Peptide Hydrogel," *Soft Matter* 7 (2011): 10210–10218, https://doi.org/10.1039/c1sm06261a.

19. G. Ghosh, R. Barman, J. Sarkar, and S. Ghosh, "pH-Responsive Biocompatible Supramolecular Peptide Hydrogel," *The Journal of Physical Chemistry B* 123 (2019): 5909–5915, https://doi.org/10.1021/acs.jpcb.9b02999.

20. Y. Shi, Y. Xu, L. Zhang, Y. Yan, and J. Yan, "Genetically Programmed Temperature-Responsive Barnacle-Derived Protein with an Enhanced Adhesion Ability," *ACS Applied Bio Materials* 7 (2024): 4573–4579, https://doi.org/10.1021/acsabm.4c00455.

21. Y. Li, C. Yang, S. Fang, et al., "Clickable, Thermally Responsive Hydrogels Enabled by Recombinant Spider Silk Protein and Spy Chemistry for Sustained Neurotrophin Delivery," *Advanced Materials* 37 (2025): 2413957, https://doi.org/10.1002/adma.202413957.

22. L. K. Hill, M. Meleties, P. Katyal, et al., "Thermoresponsive Protein-Engineered Coiled-Coil Hydrogel for Sustained Small Molecule Release," *Biomacromolecules* 20 (2019): 3340–3351, https://doi.org/10.1021/acs.biomac.9b00107.

23. Y. Mizuguchi, Y. Mashimo, M. Mie, and E. Kobatake, "Temperature-Responsive Multifunctional Protein Hydrogels with Elastin-Like Polypeptides for 3-D Angiogenesis," *Biomacromolecules* 21 (2020): 1126–1135, https://doi.org/10.1021/acs.biomac.9b01496.

24. T. Duan, Q. Bian, and H. Li, "Light-Responsive Dynamic Protein Hydrogels Based on LOVTRAP," *Langmuir* 37 (2021): 10214–10222, https://doi.org/10.1021/acs.langmuir.1c01699.

25. R. Wang, Z. Yang, J. Luo, I.-M. Hsing, and F. Sun, "B12-Dependent Photoresponsive Protein Hydrogels for Controlled Stem Cell/Protein Release," *Proceedings of the National Academy of Sciences* 114 (2017): 5912–5917, https://doi.org/10.1073/pnas.1621350114.

26. J. Lei and H. Li, "The Photocleavable Protein PhoCl-Based Dynamic Hydrogels," *ACS Biomaterials Science & Engineering* 10 (2024): 7404–7412, https://doi.org/10.1021/acsbiomaterials.4c01584.

27. N. E. Gregorio, F. Zhang, Y. Suita, et al., "PhoCoil: A Photodegradable and Injectable Single-component Recombinant Protein Hydrogel for Minimally Invasive Delivery and Degradation," *Science Advances* 11 (2025): adx3472, https://doi.org/10.1126/sciadv.adx3472.

28. Q. Bian, N. Kong, S. Arslan, and H. Li, "Calmodulin-Based Dynamic Protein Hydrogels with Three Distinct Mechanical Stiffness," *Advanced Functional Materials* 34 (2024): 2404934, https://doi.org/10.1002/adfm.202404934.

29. N. E. Gregorio, Z. Li, J. W. Hoye, D. Baker, and C. A. DeForest, "Stimuli-Triggered Formation of De Novo-Designed Protein Biomaterials," *Cell Biomaterials* 2 (2025): 100239, https://doi.org/10.1016/j.celbio.2025.100239.

30. M.-L. Zhou, Z.-G. Qian, L. Chen, D. L. Kaplan, and X.-X. Xia, "Rationally Designed Redox-Sensitive Protein Hydrogels with Tunable Mechanical Properties," *Biomacromolecules* 17 (2016): 3508–3515, https://doi.org/10.1021/acs.biomac.6b00973.

31. S. Jia, J. Wang, X. Wang, et al., "Genetically Encoded in Situ Gelation Redox-Responsive Collagen-Like Protein Hydrogel for Accelerating Diabetic Wound Healing," *Biomaterials Science* 11 (2023): 7748–7758, https://doi.org/10.1039/D3BM01010D.

32. B. A. Badeau, M. P. Comerford, C. K. Arakawa, J. A. Shadish, and C. A. DeForest, "Engineered Modular Biomaterial Logic Gates for Environmentally Triggered Therapeutic Delivery," *Nature Chemistry* 10 (2018): 251–258, https://doi.org/10.1038/nchem.2917.

33. B. A. Badeau and C. A. DeForest, "Programming Stimuli-Responsive Behavior into Biomaterials," *Annual Review of Biomedical Engineering* 21 (2019): 241–265, https://doi.org/10.1146/annurev-bioeng-060418-052324.

34. R. Gharios, M. L. Ross, A. Li, S. P. Kottantharayil, J. Hoye, and C. A. DeForest, "Boolean Logic-Gated Protein Presentation Through Autonomously Compiled Molecular Topology," *Nature Chemical Biology* 21 (2025): 1981–1991, https://doi.org/10.1038/s41589-025-02037-5.

35. M. L. Ross, R. Gharios, S. Kottantharayil, A. Li, and C. A. DeForest, "Boolean Logic-Based Controlled Release of Bioactive Proteins with Diversified Inputs," *Angewandte Chemie International Edition* 64 (2025): 19925, https://doi.org/10.1002/anie.202519925.

36. B. M. Dorr, H. O. Ham, C. An, E. L. Chaikof, and D. R. Liu, "Reprogramming the Specificity of Sortase Enzymes," *Proceedings of the National Academy of Sciences* 111 (2014): 13343–13348, https://doi.org/10.1073/pnas.1411179111.

37. E. H. Abdelkader and G. Otting, "NT*-HRV3CP: an Optimized Construct of human Rhinovirus 14 3C Protease for High-yield Expression and Fast Affinity-tag Cleavage," *Journal of Biotechnology* 325 (2021): 145–151, https://doi.org/10.1016/j.jbiotec.2020.11.005.

38. L. D. Cabrita, D. Gilis, A. L. Robertson, Y. Dehouck, M. Rooman, and S. P. Bottomley, "Enhancing the Stability and Solubility of TEV Protease Using in Silico Design," *Protein Science* 16 (2007): 2360–2367, https://doi.org/10.1110/ps.072822507.

39. A. H. Keeble, V. K. Yadav, M. P. Ferla, et al., "DogCatcher Allows Loop-friendly Protein-protein Ligation," *Cell Chemical Biology* 29 (2022): 339–350.e10, https://doi.org/10.1016/j.chembiol.2021.07.005.

40. X. Gao, J. Fang, B. Xue, L. Fu, and H. Li, "Engineering Protein Hydrogels Using SpyCatcher-SpyTag Chemistry," *Biomacromolecules* 17 (2016): 2812–2819, https://doi.org/10.1021/acs.biomac.6b00566.

41. F. Sun, W.-B. Zhang, A. Mahdavi, F. H. Arnold, and D. A. Tirrell, "Synthesis of Bioactive Protein Hydrogels by Genetically Encoded SpyTag-SpyCatcher Chemistry," *Proceedings of the National Academy of Sciences* 111 (2014): 11269–11274, https://doi.org/10.1073/pnas.1401291111.

42. B. Zakeri, J. O. Fierer, E. Celik, et al., "Peptide Tag Forming a Rapid Covalent Bond to a Protein, Through Engineering a Bacterial Adhesin," *Proceedings of the National Academy of Sciences* 109 (2012): E690–E697, https://doi.org/10.1073/pnas.1115485109.

43. T. Xu, Y. Sun, Y.-X. Wang, et al., "A High Modulus, Multi-Stimuli Responsive, Interwoven Protein Network with Topologically Confined Micro-Association," *Angewandte Chemie International Edition* 64 (2025): 202516010, https://doi.org/10.1002/anie.202516010.

44. B. C. Campbell, E. M. Nabel, M. H. Murdock, et al., "mGreenLantern: a Bright Monomeric Fluorescent Protein with Rapid Expression and Cell Filling Properties for Neuronal Imaging," *Proceedings of the National Academy of Sciences* 117 (2020): 30710–30721, https://doi.org/10.1073/pnas.2000942117.

45. A. J. Stevens, Z. Z. Brown, N. H. Shah, G. Sekar, D. Cowburn, and T. W. Muir, "Design of a Split Intein with Exceptional Protein Splicing Activity," *Journal of the American Chemical Society* 138 (2016): 2162–2165, https://doi.org/10.1021/jacs.5b13528.

46. R. E. Thompson, A. J. Stevens, and T. W. Muir, "Protein Engineering Through Tandem Transamidation," *Nature Chemistry* 11 (2019): 737–743, https://doi.org/10.1038/s41557-019-0281-2.

47. J. E. Townend and A. Tavassoli, "Traceless Production of Cyclic Peptide Libraries in *E. coli*," *ACS Chemical Biology* 11 (2016): 1624–1630, https://doi.org/10.1021/acschembio.6b00095.

48. G. Veggiani, T. Nakamura, M. D. Brenner, et al., "Programmable Polyproteams Built Using Twin Peptide Superglues," *Proceedings of the National Academy of Sciences* 113 (2016): 1202–1207, https://doi.org/10.1073/pnas.1519214113.

49. Q. Xu, D. Ming, C. Shi, et al., "Catcher/Tag Cyclization Introduces Electrostatic Interaction Mediated Protein-Protein Interactions to Enhance the Thermostability of Luciferase," *Process Biochemistry* 80 (2019): 64–71, https://doi.org/10.1016/j.procbio.2019.02.008.

50. F. Sun and W.-B. Zhang, "Genetically Encoded Click Chemistry†," *Chinese Journal of Chemistry* 38 (2020): 894–896, https://doi.org/10.1002/cjoc.202000101.

51. I. C. Jenkins, J. J. Milligan, and A. Chilkoti, "Genetically Encoded Elastin-Like Polypeptides for Drug Delivery," *Advanced Healthcare Materials* 10 (2021): 2100209, https://doi.org/10.1002/adhm.202100209.

52. Z. Dai, X. Yang, F. Wu, et al., "Living Fabrication of Functional Semi-interpenetrating Polymeric Materials," *Nature Communications* 12 (2021): 3422, https://doi.org/10.1038/s41467-021-23812-7.

53. D. Asai, D. Xu, W. Liu, et al., "Protein Polymer Hydrogels by In Situ, Rapid and Reversible Self-gelation," *Biomaterials* 33 (2012): 5451–5458, https://doi.org/10.1016/j.biomaterials.2012.03.083.

54. K. Lee, Y. Noh, Y. Bae, S. Kang, and C. Cha, "Tunable Physicomechanical and Drug Release Properties of In Situ Forming Thermoresponsive Elastin-like Polypeptide Hydrogels," *Biomacromolecules* 23 (2022): 5193–5201, https://doi.org/10.1021/acs.biomac.2c01001.

55. S. G. Martinusen, S. E. Nelson, E. W. Slaton, et al., "Protease Engineering: Approaches, Tools, and Emerging Trends," *Biotechnology Advances* 82 (2025): 108602, http://doi.org/10.1016/j.biotechadv.2025.108602.

56. R. P. Dyer and G. A. Weiss, "Making the Cut with Protease Engineering," *Cell Chemical Biology* 29 (2022): 177–190, https://doi.org/10.1016/j.chembiol.2021.12.001.

57. S. Dolati, M. Yousefi, A. Pishgahi, S. Nourbakhsh, B. Pourabbas, and S. K. Shakouri, "Prospects for the Application of Growth Factors in Wound Healing," *Growth Factors* 38 (2020): 25–34, https://doi.org/10.1080/08977194.2020.1820499.

58. S. H. Shin, Y. G. Koh, W. G. Lee, J. Seok, and K. Y. Park, "The Use of Epidermal Growth Factor in Dermatological Practice," *International Wound Journal* 20 (2022): 2414–2423, https://doi.org/10.1111/iwj.14075.

59. N. Yamaguchi, L. Zhang, B.-S. Chae, C. S. Palla, E. M. Furst, and K. L. Kiick, "Growth Factor Mediated Assembly of Cell Receptor-Responsive Hydrogels," *Journal of the American Chemical Society* 129 (2007): 3040–3041, https://doi.org/10.1021/ja0680358.

60. B.-H. Shan and F.-G. Wu, "Hydrogel-Based Growth Factor Delivery Platforms: Strategies and Recent Advances," *Advanced Materials* 36 (2024): 2210707, https://doi.org/10.1002/adma.202210707.

61. L. L.-W. Wang, Y. Gao, Z. Feng, D. J. Mooney, and S. Mitragotri, "Designing Drug Delivery Systems for Cell Therapy," *Nature Reviews Bioengineering* 2 (2024): 944–959, https://doi.org/10.1038/s44222-024-00214-0.

62. A. A. Abdeen and K. Saha, "Manufacturing Cell Therapies Using Engineered Biomaterials," *Trends Biotechnology* 35 (2017): 971–982, https://doi.org/10.1016/j.tibtech.2017.06.008.

63. A. A. Dravid, A. Singh, and A. J. García, "Biomaterial-Based Therapeutic Delivery of Immune Cells," *Advanced Healthcare Materials* 14 (2025): 2400586, https://doi.org/10.1002/adhm.202400586.

64. M. E. Matlashov, D. M. Shcherbakova, J. Alvelid, et al., "A Set of Monomeric near-infrared Fluorescent Proteins for Multicolor Imaging Across Scales," *Nature Communications* 11 (2020): 239, https://doi.org/10.1038/s41467-019-13897-6.

65. J. Despanie, J. P. Dhandhukia, S. F. Hamm-Alvarez, and J. A. MacKay, "Elastin-Like Polypeptides: Therapeutic Applications for an Emerging Class of Nanomedicines," *Journal of Controlled Release* 240 (2016): 93–108, https://doi.org/10.1016/j.jconrel.2015.11.010.

66. J. Cui, Y. Gao, C. Lu, et al., "Engineering a Thermally Activatable SpyCatcher/SpyTag Protein Ligation for Injectable and In Situ-Forming Hydrogels," *Angewandte Chemie International Edition* 65 (2026): 09477, https://doi.org/10.1002/anie.202509477.

Supporting Information

Additional supporting information can be found online in the Supporting Information section.

Supporting File: adma74038-sup-0001-SuppMat.pdf.